## Polymetamorphism and ductile deformation of staurolite-cordierite schist of the Bossost Dome: indication for Variscan extension in the Axial Zone of the central Pyrenees

Mezger, J.E.; Passchier, C.W.

***published in***
Geological Magazine
2003

***DOI (link to publisher)***
10.1017/S0016756803008112

***document version***
Publisher's PDF, also known as Version of record

*Geol. Mag.* **140** (*5*), *2003, pp. 595–612.* © *2003 Cambridge University Press*
DOI: 10.1017/S0016756803008112 *Printed in the United Kingdom*


# Polymetamorphism and ductile deformation of staurolite–cordierite schist of the Bossòst dome: indication for Variscan extension in the Axial Zone of the central Pyrenees

JOCHEN E. MEZGER* & CEES W. PASSCHIER

Johannes Gutenberg-Universität, Institut für Geowissenschaften, Becherweg 21, 55099 Mainz, Germany

(*Received* 12 August 2002; *accepted* 9 June 2003)

**Abstract** – The Bossòst dome is an E–W-trending elongated structural and metamorphic dome developed in Cambro-Ordovician metasedimentary rocks in the Variscan Axial Zone of the central Pyrenees. A steep fault separates a northern half-dome, cored by massif granite, from an E–W-trending doubly plunging antiform with granitic sills and dykes in the core to the south. The main foliation is a flat-lying $S_{1/2}$ schistosity that grades into a steeper-dipping slaty cleavage at the dome margins. Three major deformational and two metamorphic phases can be differentiated. $S_{1/2}$ schistosity is an axial planar cleavage to W-vergent recumbent folding that probably occurred in mid-Westphalian time. Peak regional metamorphism $M_1$ is characterized by static growth of staurolite and garnet following thermal relaxation of the previously thickened crust. Strong non-coaxial deformation recording uniform top-to-the-SE extension during $D_{2a}$ is preserved in staurolite–garnet schists in a 1.5 km thick, shallowly SE-dipping zone in the southeastern dome. A 500 m thick contact aureole ($M_2$) was imprinted on the regionally metamorphosed rocks following the intrusion the Bossòst granite during $D_{2b}$. More coaxial deformation prevailed during synkinematic growth of $M_2$ phases in the inner part of the contact aureole around the northern part of the dome, where it obliterated $D_{2a}$ fabrics. Progressive non-coaxial deformation continued in the southeastern antiform and is recorded by late-synkinematic growth of cordierite. Successive overprinting of the $M_1$ staurolite–garnet assemblage by andalusite and cordierite of $M_2$ is preserved in the southern part. The assemblage muscovite + cordierite + staurolite + biotite is considered metastable, given the low Mn and Zn contents of staurolite and cordierite, and interpreted as the result of prograde metamorphism during decompression. *P–T* conditions during $M_2$ were approximately 3 kbar and 600 °C. Pervasive crenulations and mesoscopic to regional southerly verging folds are the result of $D_3$ NNE–SSW compression post-dating ductile deformation and contact metamorphism. Polymetamorphic assemblages of the Bossòst dome preserve a regionally confined zone of ESE-directed extensional shearing within an overall N–S compressional setting. Exact timing of extensional shearing is not known, but can be constrained by recumbent folding during the mid-Westphalian and granitic intrusions, which confine it to Late Carboniferous time (*c*. 305 Ma). Crustal-scale flat-lying extensional shear zones with similar orientation and time frame are observed in the Hospitalêt massif of the eastern Axial Zone. This suggests that crustal extension, though probably restricted by regional strain partitioning over orthogneiss or intruding granitic bodies within an overall compressive setting, was not uncommon in Late Carboniferous time in the Axial Zone of the Pyrenees.

Keywords: contact metamorphism, ductile deformation, extension tectonics, Variscan, Pyrenees.

## 1. Introduction

Elongated structural and metamorphic domes are a common feature in the cores of orogenic belts (Eskola, 1949; Teyssier & Whitney, 2002). They are characterized by alignment of their long axes parallel to the trend of the orogenic belt and gneissic or migmatitic cores mantled by deformed metasedimentary rocks. In the marginal zones, low-grade metamorphic rocks commonly have a steep-dipping foliation, whereas high-grade rocks near the core of the dome commonly display a shallow-dipping foliation. The tectonic models evoked for dome development fall into four broader categories: (1) compression, which includes the diapirism (Ramberg, 1980; Soula, 1982) and transpression (Carreras & Capella, 1994; Gleizes, Leblanc & Bouchez, 1997) models; (2) extension, which comprises models of crustal thinning in an extensional setting, known as metamorphic core complexes (Lister & Davis, 1989; Malavielle *et al.* 1990; Oliver, 1994; Hetzel *et al.* 1995; Dirks, Zhang & Passchier, 1997) and coupled crustal thinning and diapirism (Teyssier & Whitney, 2002); (3) a combination of compression followed by extension or doming (Zwart, 1986; Gibson, 1989, 1991; Aerden, 1994, 1998); and (4) interference of polyphase intrusions with large-scale folds and flat-lying shear zones (Passchier, 1994; Myers, 1995; Zegers *et al.* 1998).

* Author for correspondence: mezger@uni-mainz.de

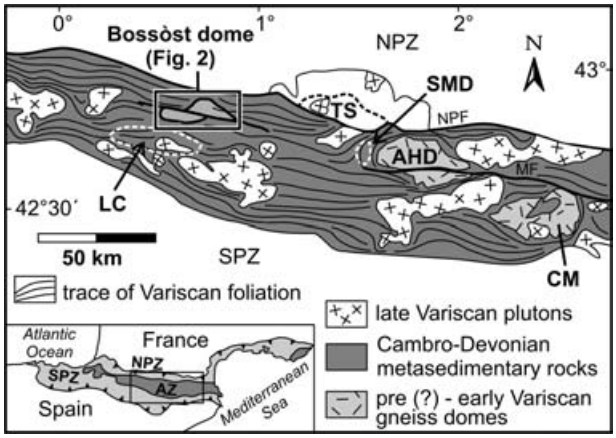


Figure 1. Sketch map of the Eastern Pyrenees displaying the three tectonic elements of the Axial Zone (AZ) and the trace of Variscan foliation. AHD – Aston-Hospitalêt dome; CM – Canigou massif; LC – Lys-Caillaouas massif; MF – Merens Fault; NPF – North Pyrenean Fault; NPZ – North Pyrenean Zone; SPZ – South Pyrenean Zone; SMD – Soulcem metamorphic dome; TS – Trois Seigneurs massif. Modified after van den Eeckhout & Zwart (1988) and Gleizes, Leblanc & Bouchez (1997).

The Variscan Axial Zone of the Pyrenees is an excellent area to study structural and metamorphic domes. The Pyrenean domes are seated in Cambro-Ordovician metasedimentary rocks, where the steep foliation of a suprastructure was overprinted at deeper structural levels by flat-lying schistosities that form an infrastructure (Carreras & Capella, 1994). Low-pressure regional metamorphism coincided with development of the infrastructure and reached upper amphibolite facies. The core zones are composed of Late Carboniferous granitic intrusions (Trois Seigneurs, Lys-Caillaouas, Bossòst) or Ordovician orthogneisses (Aston-Hospitalêt, Canigou).

The interpretations of complex microstructures and growth of metamorphic porphyroblasts in the domes resulted in conflicting views on the relative timing of regional metamorphism and infrastructure development. In the Trois Seigneurs massif (Fig. 1), porphyroblasts are obliquely transected by rotation of the external foliation during non-coaxial sinistral flow, suggesting that the infrastructure is younger than regional metamorphism (Passchier & Speck, 1994). Other authors proposed regional metamorphism and granite emplacement coeval with dextral transpression (Leblanc *et al.* 1996). In the Lys-Caillaouas massif further west (Fig. 1), regional metamorphism is closely related to formation of a subhorizontal crenulation cleavage during ESE–WNW non-coaxial extension (de Bresser, Majoor & Ploegsma, 1986; Kriegsman *et al.* 1989; Aerden, 1994). Narrow contact aureoles around late Variscan granite intrusions indicate that they post-date regional metamorphism. The Canigou massif in the eastern Pyrenees (Fig. 1) is an easterly plunging antiformal structure defined by a core of late Variscan granites overlain by Cambro-Ordovician schists interlayered with an orthogneiss, an early Ordovician laccolith which intruded the Cambrian sediments prior to Variscan deformation (Barbey, Cheilletz & Laumonier, 2001; Deloule *et al.* 2002). Gibson (1989) proposed that the flat-lying foliation resulted from non-coaxial extension with top-to-the-NW sense of shear. Laumonier & Autran (2001) postulated the presence of only one schistosity, which was steepened by a late Variscan S-directed thrust, whose footwall forms the infrastructure, while the steep-dipping foliation of the hanging wall represents the suprastructure.

The largest domal structures in the Axial Zone are the Aston and Hospitalêt domes (Fig. 1). The two adjacent domes, which are separated by the narrow E-trending Merens Fault, consist of large orthogneiss cores that intruded Cambro-Ordovician metasediments prior to development of the main flat-lying infrastructure, which transposed the steep E–W-striking axial planar cleavage of the suprastructure. Peak-metamorphism occurred after development of the infrastructure, evident from migmatization at the base of the western Aston orthogneiss (Verhoef, Vissers & Zwart, 1984). The infrastructure of the Hospitalêt dome is interpreted as a crustal-scale extensional shear zone developed at the gneiss–schist contact (van den Eeckhout & Zwart, 1988). The small Soulcem metamorphic dome (Fig. 1) overprinted regional metamorphic isograds around the western margin of the Aston orthogneiss, and is related to small granitic intrusions that are exposed in the core. Vissers (1992) interprets the Soulcem metamorphic dome as the result of thermally induced ductile collapse of steep structures with ESE–WNW-directed extension.

With rapid advancements in the understanding of microstructures and metamorphic phase relations in the last decade, we have chosen to reinvestigate one of the more prominent metamorphic and structural domes, the Bossòst dome, also known as the Garonne dome, the site of Zwart's (1962) landmark study on the relationship of porphyroblast growth and deformation. Pouget (1991) postulated a diapric origin of the Bossòst dome, but the geothermobarometric calculations essential for his model were contested (Gibson, 1992), so that the tectonic evolution of the Bossòst dome remained a matter of conjecture. We present detailed microstructural and petrological analyses that reveal the complex interaction of deformational and metamorphic events.

## 2. Geological overview

The Bossòst dome is one of the smaller domes in the Axial Zone of the Pyrenees. It is approximately 35 km long and 15 km wide, and its long axis is aligned to the trend of the Axial Zone (Fig. 1). To the north, the

Northern Pyrenean Fault separates it from the North Pyrenean Zone and, to the south, the Aran Valley synclinorium separates it from the Lys-Caillaouas dome and the Maladeta pluton (Garcia-Sansegundo, 1996). The Bossòst dome itself is transected by the E–W-trending Bossòst Fault (Calembert, 1951), which is interpreted as part of orogen-parallel Alpine mylonite zones and a continuation of the Merens Fault further to the east (Fig. 1, C. Lamouroux, unpub. Ph.D. thesis, Univ. Toulouse, 1987).

The core of the dome consists of fine- to medium-grained, massive, leucocratic muscovite–hornblende granites, and minor two-mica granites (Fig. 2). In the northern section granitic rocks form a roughly triangular core with sides 3–4 km long, truncated to the south by the Bossòst Fault. Outside the core zone the granitic rocks form apophyses or discontinuous, decimetre- to metre-thick sills and dykes. South of the Bossòst Fault granitic intrusions occur as smaller, elongated, E–W-aligned bodies. The contact between granite and schist is intrusive, generally cross-cutting a pre-existing schistosity. The intrusive age of the Bossòst granitoids is not known, but from the lack of internal deformation and ductile fabrics they can be correlated with other late Variscan granitic massifs in the Axial Zone, such as Bassiès (312 Ma) and Mont Louis-Andorra (305 Ma) plutons (Gleizes, Leblanc & Bouchez, 1997). A foliated quartz diorite with no clear relation to the main granitic body and of unknown age has been observed close to the core (Fig. 2).

Mantling the granites are mica–quartz schists with intercalated minor micaceous quartzites and quartzites of Cambro-Ordovician age (Zwart, 1963; Garcia-Sansegundo, 1996). The schists are dark bluish grey, fine-grained with a high quartz content (> 60 vol. %) and possess a continuous schistosity. Andalusite, fibrous sillimanite, garnet, staurolite and cordierite may be present. Common accessory minerals are ilmenite, zircon, tourmaline, apatite and minor graphite. Feldspars are conspicuously rare. Chlorite and sericite are common alteration phases. Along the eastern contact of the granite, near the peak of Montlude, migmatized metasedimentary rocks are observed. Towards the margins of the dome the schists grade successively into phyllites and finely laminated dark grey, quartz-rich slates at distances of more than 2 km from the intrusion.

Overlying the Cambro-Ordovician schists and slates to the east is an Ordovician coarse-crystalline, bluish white marble with compositional banding (Bartholomé, 1953). Marble caps ridges in the eastern parts of the Bossòst dome, whereas in the southeast it forms a narrow, discontinuous, N-striking band overlain by brown-weathering, dark carbonaceous Silurian slate (de Sitter & Zwart, 1960). In the western part of the Bossòst dome, Cambro-Ordovician slate is directly overlain by Silurian slate, which has a thickness of 10–100 m and is interfolded with overlying Devonian bluish grey, quartz-rich slates and dark marble (de Sitter & Zwart, 1960). The Devonian rocks are generally of low metamorphic grade, but contain staurolite and andalusite in the Garona valley near es Bordes (Fig. 2). Pouget (1991) reported the presence of chloritoid along the southeastern margin of the dome.

The main foliation within the Bossòst dome is a flat-lying schistosity in the core zone and a steeper foliation along the marginal areas and in the overlying post-Ordovician rocks. While Zwart (1962, 1963) proposed that shallow and steep foliations developed simultaneously during N–S shortening, Matte (1969) interpreted the steep foliation as refolding of the original flat-lying schistosity. East of the Bossòst dome, Garcia-Sansegundo & Alonso (1989) proposed that the flat-lying foliation is a crenulation cleavage associated with N-verging kilometre-scale recumbent folds. The tightly folded Devonian cover units have moved southward over a décollement located at the base of the Silurian black slates (Zwart, 1962; Matte & Xu Zhi, 1988; Garcia-Sansegundo, 1996). Pouget (1991) interpreted the flat-lying foliation ($S_2$) as the result of diapiric rise of the migmatitic and granitic core of the Bossòst dome in an extensional setting, which overprinted an original steeper foliation ($S_1$), forming a $D_2$ structural dome. He recognized narrow $D_3$ structural domes developed locally around individual intrusions during horizontal shortening, and a steeply S-dipping $S_4$ crenulation cleavage, which grades into $S_1$ outside the $D_2$ structural dome. Garcia-Sansegundo & Alonso (1989) suggested that the domal shape resulted from interference of E- and SSE-trending upright folds of the main foliation.

Bartholomé (1953) associated metamorphic assemblages in the metasedimentary rocks of the core of the Bossòst dome with contact metamorphism. Zwart (1962), in his landmark study of the interaction of deformation and porphyroblast growth, described four metamorphic zones corresponding to four deformation phases. He suggested that regional metamorphism was related to metasomatism at a very low pressure (*c*. 1 kbar) and that the granitic core resulted from *in situ* granitization. Pouget (1991) distinguished a biotite, an andalusite and a sillimanite zone resulting from a diapirism-related early medium-*P*–high-*T* regional metamorphism with anatexis of metasedimentary rocks and a LP contact metamorphism related to the intrusion of the granite.

Our observations show that two distinct metamorphic events occurred after formation of the main foliation. A medium-*P*–medium-*T* regional metamorphism was followed by low-*P*–high-*T* contact metamorphism, related to granitic intrusion. The two metamorphic events are divided by a period of strong non-coaxial deformation in an extensional setting and distinguished by polymetamorphic assemblages. The domal shape resulted from later NNE–SSW compression that formed local to regional folds.

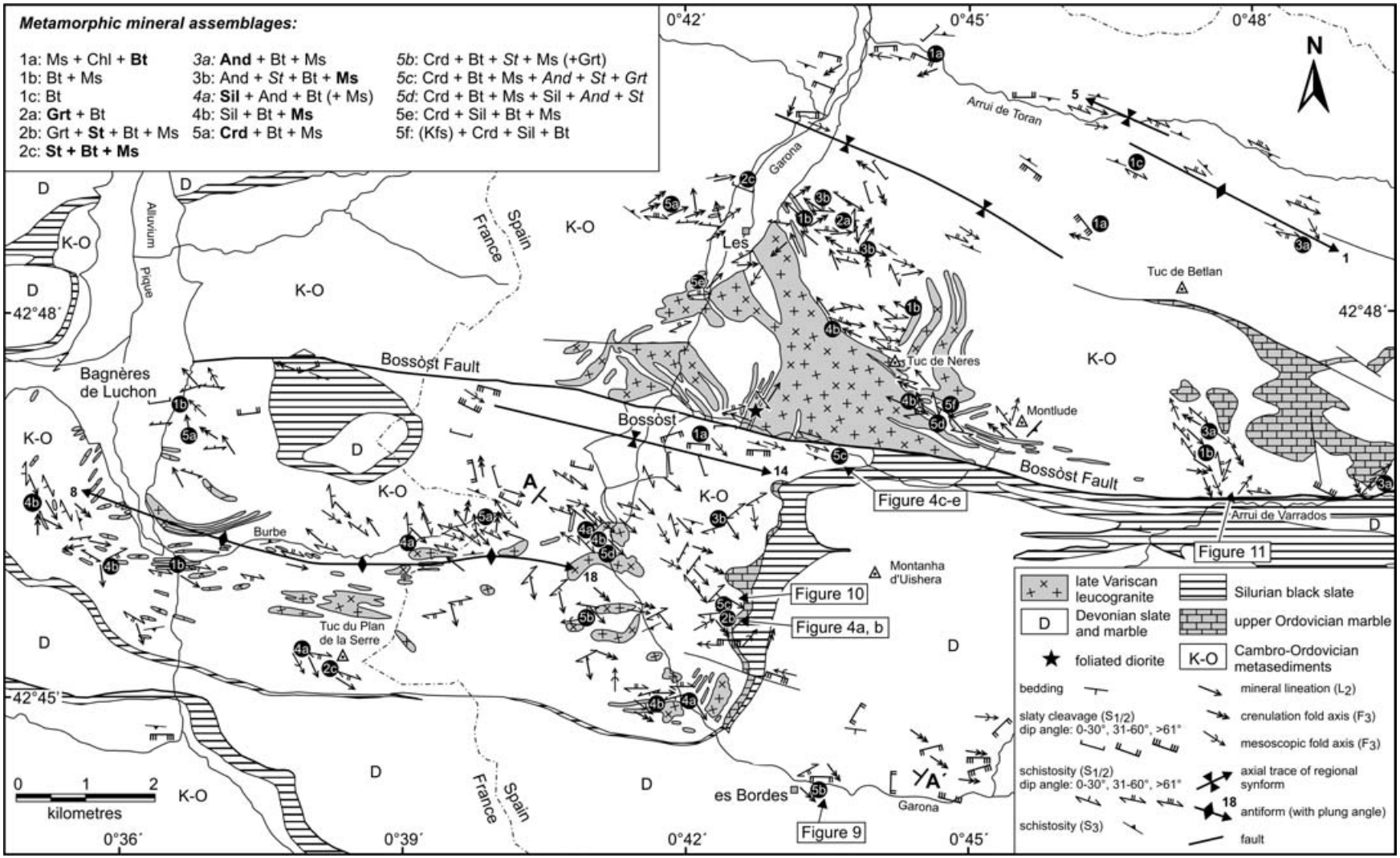


Figure 2. Structural map of the Bossòst dome with location of metamorphic mineral assemblages. Letters in bold and italics indicate first appearance and disappearance of phases, respectively. Assemblage numbers in italics indicate metastable assemblages. Mineral abbreviations follow Kretz (1983). Location of cross-section in Figure 8 (A–A′) is shown. Geology is modified after de Sitter & Zwart (1960).

## 3. Deformational phases

### 3.a. Pre-$D_1$

Millimetre- to centimetre-scale alternation of pelitic and quartz-rich layers, generally transposed into parallelism with the main schistosity, are remnants of an older foliation, which may be tectonic or an original sedimentary bedding of the Cambro-Ordovician sediments. Aluminium-rich phases, such as andalusite and staurolite, are commonly concentrated in pelitic layers, and compositional banding is reflected in different abundances of inclusions in large porphyroblasts. Rare crenulated quartz inclusion trails in spessartine-rich garnets preserve a foliation pre-dating the main schistosity.

### 3.b. $D_1$

#### *3.b.1. $S_{1/2}$ foliation*

The main foliation is a spaced or continuous foliation defined, with increasing metamorphic grade, by chlorite, muscovite and biotite. The change from slaty cleavage to schistosity is transitional and does not involve a structural break. This can be observed along a N–S transect east of Les, where muscovite–chlorite slate grades into high-grade cordierite–sillimanite–biotite schist near the intrusive contact (Fig. 2). Rootless isoclinally folded quartz layers preserved in younger andalusite porphyroblasts indicate that the main foliation is an axial planar cleavage resulting from considerable shortening of a pre-$D_1$ foliation. Biotite, garnet and staurolite porphyroblasts contain straight inclusion trails that are oriented at various angles with the external foliation ($S_e$, Fig. 4a). In some large staurolite porphyroblasts, the internal foliation ($S_i$) continues into $S_e$ (Fig. 4b), indicating that the main foliation lasted throughout later $D_2$ deformation and can be referred to as $S_{1/2}$. Our $S_{1/2}$ correlates with that of Matte (1969) and $S_2$ of Garcia-Sansegundo & Alonso (1989) and Pouget (1991).

The orientation of $S_{1/2}$ differs in the two parts of the Bossòst dome. The northern section is characterized by a broad circular maximum of moderately N- to NE-dipping schistosity in higher grade rocks, and a SSW-dipping slaty cleavage in lower grade rocks (Figs 2, 3). Strike orientations change from E, west of the Garona river, to SSE in the eastern part of the dome. Minor deflections of $S_{1/2}$ are observed adjacent to granitic bodies. The dip angle increases from 20–35° near the core to about 70° along the northeastern margin, resulting in steeper dips of the foliation in lower grade rocks (Figs 2, 3). South of the Bossòst Fault, $S_{1/2}$ dip angles range from subvertical in low grade rocks to subhorizontal in some schists, tracing an elongated, ESE-trending, doubly plunging antiform with a southerly vergence. In a stereogram, $S_{1/2}$ data form a continuous girdle around a shallowly ESE-plunging fold axis (Fig. 3).

Matte (1969), García-Sansegundo & Alonso (1989) and García-Sansegundo (1996) proposed that $S_{1/2}$ is the axial planar cleavage to large SW- and N-verging recumbent folds they observed in lower grade Cambro-Ordovician and younger slates west and east of our study area. Similar observations were made south of the Maladeta granite (Evans *et al.* 1998) and in the Pic du Midi d'Ossau–Col du Somport region of the western Axial Zone (Matte, 2002).

#### *3.b.2. $M_1$ regional metamorphism*

The lowest metamorphic grade is observed at the northern margin of the study area, near the confluence of the Arrui de Toran with the Garona river and immediately south of the Bossòst Fault. A fine-grained (*c.* 100 $\mu$m) muscovite–chlorite–quartz slate with minor biotite (assemblage 1a) grades south- and eastward into a phyllite with increasing abundance of biotite and the disappearance of primary chlorite (assemblage 1b). Locally, biotite is the only phyllosilicate observed (assemblage 1c). Large biotite porphyroblasts with quartz inclusion trails oblique to $S_{1/2}$ are truncated by smaller biotite and muscovite grains parallel to $S_{1/2}$ in the cleavage domains, suggesting that the biotite porphyroblasts grew prior to $D_2$ overprinting $S_1$ (Fig. 4d). The two biotite generations do not differ in composition, which could be the result of re-equilibration during final cooling.

Garnet, though not a very common occurrence, forms subhedral to euhedral porphyroblasts with straight quartz inclusion trails and may compose up to 5 % of the rock volume. In rocks with co-existing cordierite, which formed during the later $M_2$ event, garnets display distinct bell-shaped chemical zoning patterns. Fe increases from core to rim ($X_{alm}$ 52–60 to 66), while Mn decreases ($X_{sps}$ 25–35 to 20). Mg ($X_{prp}$ 9) and Ca ($X_{grs}$ 4–6) distribution is weakly zoned (Fig. 5, Table 1). Garnet inclusions in staurolite and cordierite do not show textural signs of rim corrosion, and little chemical resorption was revealed by electron microprobe. In contrast, garnets of a cordierite-absent staurolite schist (00–165) contain more Fe ($X_{alm}$ 85–88) and considerably less Mn and Mg, as well as less pronounced zoning patterns.

Spectacular examples of twinned staurolite occur in a fine-grained garnetiferous biotite–muscovite–quartz schist close to marble banks that mark the contact with Silurian rocks north of es Bordes (assemblage 2b, Fig. 4a). Staurolites are up to 1 cm long, euhedral, poikiloblastic and contain up to 40 vol. % inclusions of quartz and minor ilmenite. Muscovite grains abut staurolite crystals, but are not present as inclusions. Inclusion trails are straight. The staurolites show a similar relative enrichment in Fe and depletion in Mn,

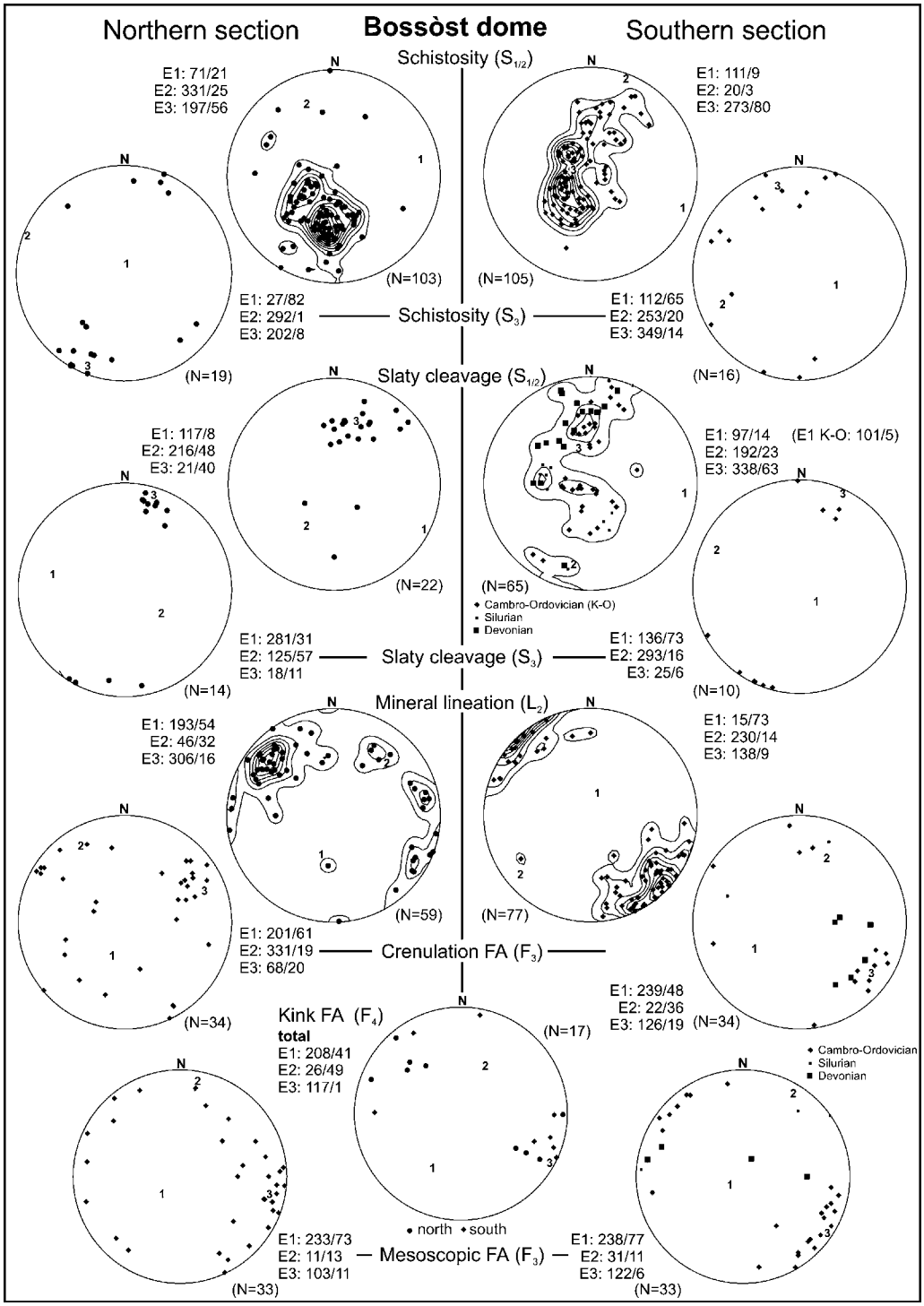


Figure 3. Equal area (Schmidt) lower hemisphere projections of the major structural fabrics of the Bossòst dome. E1, E2 and E3 represent the eigenvectors. Smoothed Gaussian contouring with contour intervals of $2\sigma$ was applied.

Mg and Zn to the garnets in this assemblage compared to staurolite in cordierite-bearing assemblages (Fig. 5, Table 1).

Chloritoid, which was reported by Pouget (1991) outside the biotite-in isograd at the southeastern margin of the Bossòst dome, was not observed in the study area. The absence of chloritoid and negligible corrosion of garnet inclusions in staurolite suggest that garnet and staurolite formation resulted from the continuous breakdown of chlorite and muscovite (reactions 1 and 2, Table 2). The garnet-forming reaction (1) occurs in the FASH system at higher temperatures than the staurolite-forming reaction, which seems inconsistent with the presence of garnet inclusions in staurolite (Fig. 13). However, the high Mn content ($X_{sps}$ 23) of garnet cores shifts the reaction (1) to lower

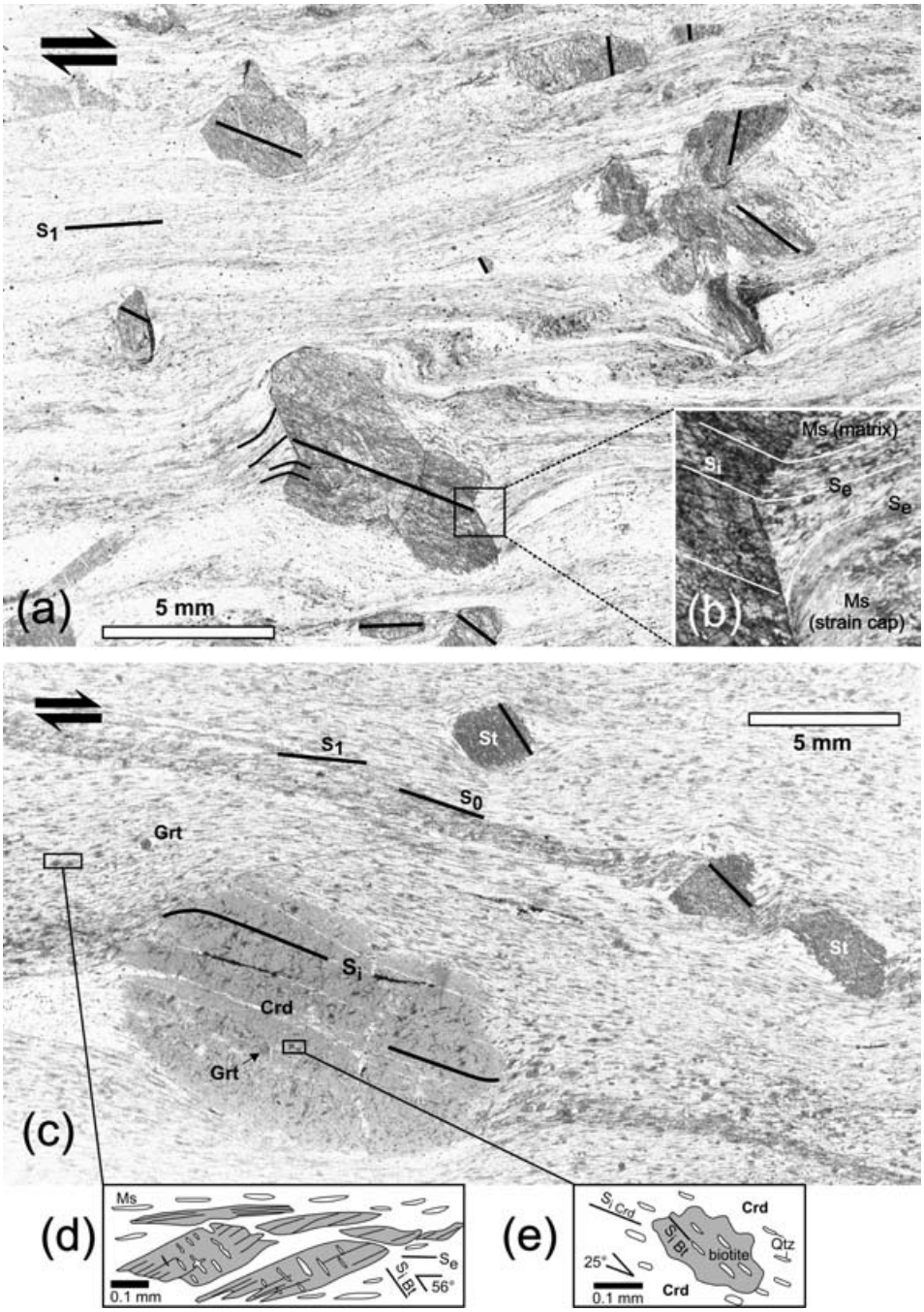


Figure 4. Scanned thin-sections from key assemblages of the southern Bossòst dome oriented parallel to the $L_2$ mineral lineation. (a) Garnet–staurolite schist of assemblage 2b, two kilometres northwest of es Bordes. Black lines trace inclusion trails in staurolite porphyroblasts. Rotated porphyroblasts indicate a dextral sense of shear. The twinned porphyroblast on the right side is broken, and its upper twin has rotated 65° clockwise with respect to the lower twin. (b) Enlarged view showing increasing obliquity between internal foliation ($S_i$) and external foliation ($S_e$) towards the muscovite strain cap. (c) Staurolite–garnet–andalusite–cordierite schist (assemblage 5c) immediately south of the Bossòst Fault. Compositional layering probably represents bedding ($S_0$) which was transposed by the main schistosity $S_{1/2}$. Angles between $S_i$ and $S_e$ are greater for staurolite (*c.* 45–55°) than for cordierite porphyroblasts (*c.* 20°). (d) Quartz inclusion trails in matrix biotite are subparallel to staurolite $S_i$. (e) $S_i$ in biotite inclusions is oriented obliquely to $S_i$ in the surrounding cordierite, but oriented parallel to $S_i$ in matrix biotite. This indicates that the biotite blast had experienced a clockwise rotation of 25° before it was overgrown by the cordierite porphyroblast and both continued rotating during its last growth phase of cordierite. The sample localities are shown on Figure 2. Abbreviations: Bt – biotite; Crd – cordierite; Grt – garnet; Ms – muscovite; Qtz – quartz; St – staurolite.

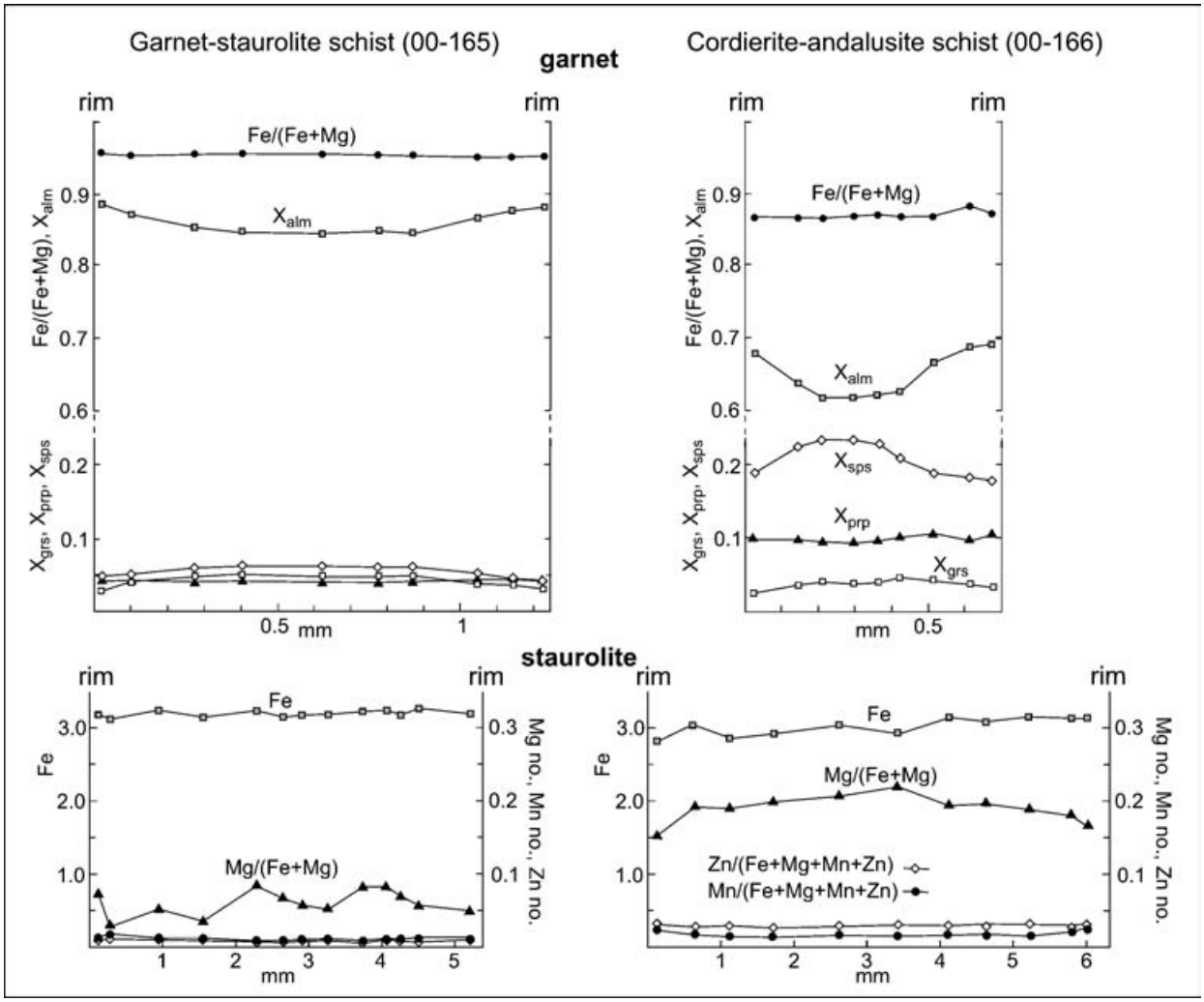


Figure 5. Compositional traverses of selected garnet and staurolite porphyroblasts. Note that the analytical data listed in Table 1 are average values of several grains.

temperatures (Spear, 1993, p. 354). On the other hand, the Fe-rich garnets ($X_{alm}$ 85) of the cordierite-absent assemblage do not appear as inclusions in staurolite, supporting nucleation after staurolite, as predicted by the petrogenetic grid (Fig. 13).

### 3.c. $D_{2a}$: non-coaxial deformation – shearing

A distinct biotite mineral lineation is developed on $S_{1/2}$, parallel to the plane of maximum fabric asymmetry. We interpret the mineral lineation to be parallel to the direction of finite strain and the direction of maximum stretching. Since the mineral lineation is absent in slate and phyllite not affected by $D_{2a}$ deformation, it can be interpreted as $L_2$. In the northern section, $L_2$ plunges shallowly towards the NW or SE, except for the northwest where NE plunge directions dominate (Fig. 3). In the southern part of the dome, $L_2$ is characterized by more uniform shallow plunges to the NW and SE.

Well-preserved staurolite porphyroblasts are restricted to the eastern part of the southern antiform, where they contain straight inclusion trails that are oriented at various angles with $S_{1/2}$ on faces parallel to $L_2$. The orientation of $S_i$ is not correlated with crystallographic axes of staurolite, indicating that the porphyroblasts statically overgrew an earlier $S_{1/2}$ fabric. The angle of obliquity of $S_i$ with $S_e$, however, is related to the orientation of $S_i$ with respect to the crystallographic axis. This angle is minimal where $S_i$ is parallel to the long axis, and maximal, that is, perpendicular to $S_e$, where $S_i$ is oriented parallel to the crystallographic short axis (Figs 4a, c, 6). Some large porphyroblasts show a continuation from $S_i$ to $S_e$ which gradually gets more oblique towards the mica strain caps (Fig. 4b). The correlation of $S_i$–$S_e$ obliquity with grain shape is evidence for non-coaxial deformation after porphyroblast growth ended, rather than static overprinting of a previous fabric asymmetry in the sense of Bell & Rubenach (1983). The amount of rotation of a blast depends on the

Table 1. Representative electron microprobe analyses of Cambro-Ordovician mica schist of the Bossòst dome

| | Garnet | | | | | | |
|---|---|---|---|---|---|---|---|
| | 00–165 | | 00–166 | | Staurolite | | Cordierite |
| Sample no. | Core | Rim | Core | Rim | 00–165 | 00–166 | 00–166 |
| *n* | 5 | 9 | 4 | 9 | 37 | 29 | 5 |
| $SiO_2$ | 36.58 | 36.60 | 36.66 | 36.75 | 26.84 | 26.61 | 48.17 |
| $TiO_2$ | 0.02 | 0.02 | 0.07 | 0.03 | 0.43 | 0.54 | 0.02 |
| $Al_2O_3$ | 21.29 | 21.27 | 21.59 | 21.63 | 55.19 | 55.07 | 31.66 |
| FeO | 36.94 | 38.47 | 27.99 | 30.13 | 13.17 | 12.30 | 8.64 |
| MnO | 2.75 | 1.94 | 10.07 | 8.42 | 0.09 | 0.47 | 0.50 |
| MgO | 0.97 | 1.06 | 2.39 | 2.41 | 0.58 | 1.59 | 7.57 |
| CaO | 1.59 | 0.98 | 1.32 | 1.19 | 0.01 | 0.01 | 0.03 |
| $Cr_2O_3$ | 0.03 | 0.04 | 0.04 | 0.03 | 0.05 | 0.05 | 0.02 |
| ZnO | 0.02 | 0.00 | 0.00 | 0.00 | 0.16 | 0.33 | – |
| Total | 100.19 | 100.37 | 100.12 | 100.59 | 96.53 | 96.96 | 97.36* |
| No. of ions based on | 12 O | | | | 48 O | | 18 O |
| Si | 2.982 | 2.983 | 2.963 | 2.960 | 7.854 | 7.749 | 5.040 |
| Ti | 0.001 | 0.001 | 0.004 | 0.002 | 0.096 | 0.119 | 0.001 |
| Al | 2.046 | 2.043 | 2.056 | 2.054 | 19.032 | 18.913 | 3.904 |
| $Fe^{2+}$ | 2.518 | 2.621 | 1.891 | 2.029 | 3.222 | 2.998 | 0.756 |
| Mn | 0.190 | 0.134 | 0.689 | 0.575 | 0.023 | 0.116 | 0.044 |
| Mg | 0.117 | 0.128 | 0.287 | 0.289 | 0.254 | 0.692 | 1.181 |
| Ca | 0.139 | 0.085 | 0.114 | 0.103 | 0.002 | 0.003 | 0.004 |
| Cr | 0.002 | 0.003 | 0.002 | 0.002 | 0.011 | 0.011 | 0.000 |
| Zn | 0.001 | 0.000 | 0.000 | 0.000 | 0.036 | 0.070 | – |
| Total | 7.997 | 7.998 | 8.008 | 8.013 | 30.529 | 30.671 | 11.082 |
| $X_{grs}$ | 0.047 | 0.029 | 0.039 | 0.034 | | | |
| $X_{prp}$ | 0.040 | 0.043 | 0.096 | 0.097 | | | |
| $X_{alm}$ | 0.850 | 0.883 | 0.634 | 0.677 | | | |
| $X_{sps}$ | 0.064 | 0.045 | 0.231 | 0.192 | | | |
| Fe/(Fe + Mg) | 0.955 | 0.953 | 0.868 | 0.875 | 0.927 | 0.813 | 0.390 |
| Mn/(Fe + Mg + Mn + Zn) | | | | | 0.007 | 0.030 | 0.030 |
| Zn/(Fe + Mg + Mn + Zn) | | | | | 0.010 | 0.018 | |

* includes 0.75 vol. % $Na_2O$. Analyses were made at the Institut für Geowissenschaften, Johannes Gutenberg-Universität Mainz, using a JEOL-JXA 8900 RL microprobe. Natural minerals were used as standards. Acceleration voltage was 20 kV (15 kV) and beam current was 20 nA (12 nA) for garnet and staurolite (cordierite). Data reduction with the CIT-ZAF software of JEOL.

original shape and orientation of the long axis with respect to the shear plane as predicted by Passchier *et al.* (1992) (Fig. 6). $D_{2a}$ did not form a new planar fabric, but reactivated a pre-existing $D_1$ schistosity.

The sense of shear obtained from rotated staurolite porphyroblasts is consistent on the sample scale and confirmed by tight folds in zones of shortening between large elongated porphyroblasts (Fig. 4a), and biotite fish with quartz inclusion trails that show the same orientation as inclusion trails in staurolite grains of the same sample (Fig. 4d). Regionally, the shear sense indicators show consistent, top-to-the-SE, hanging wall-down sense of shear (Fig. 7). While this sense of shear is observed in a 1.5 km thick zone in the eastern part of the southern antiform (Fig. 8), $D_{2a}$ non-coaxial deformation features are best preserved in a 200 m wide zone of staurolite–garnet schist along a trail northwest of the village of Arres, where it is located immediately underneath Ordovician marble and weakly metamorphosed Silurian black slate. Here, staurolite is not consumed by later $M_2$ metamorphism. In the northern section, $L_2$ is related to coaxial deformation.

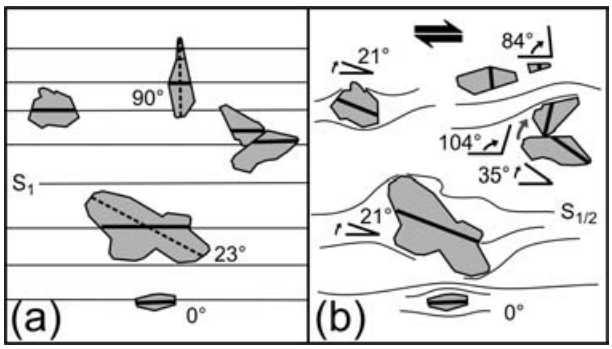


Figure 6. Sketch of staurolite porphyroblasts of Figure 4a. (a) Orientation of porphyroblasts prior to $D_{2a}$ obtained by restoring parallel alignment of $S_i$ with $S_{1/2}$. Angles of crystal length axes (dashed lines) with $S_1$ are shown. (b) Present orientation of porphyroblasts with angles between $S_i$ and $S_{1/2}$.

Non-coaxial deformation with top-to-the-SE sense of shear extends southeastwards into Devonian staurolite–andalusite–mica schist exposed near es Bordes along the Garona river valley. Curved graphitic inclusion trails indicate synkinematic growth of staurolite (Fig. 9). $\sigma$-type quartz pressure shadows

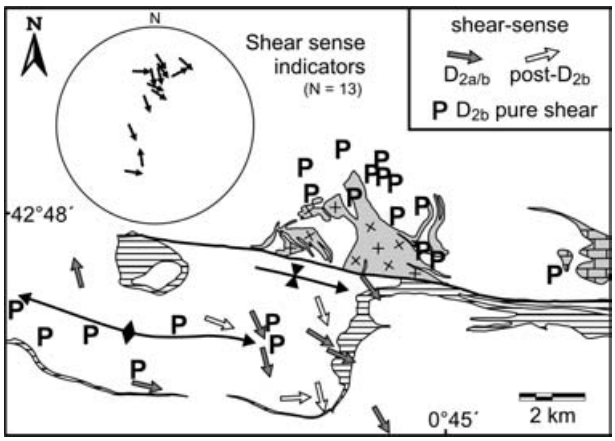


Figure 7. Map and slip linear stereographic projection of shear sense indicators in the Bossòst dome associated with $D_{2a}$, $D_{2a/b}$ and post-$D_{2b}$. Geological and structural symbols as in Figure 2.

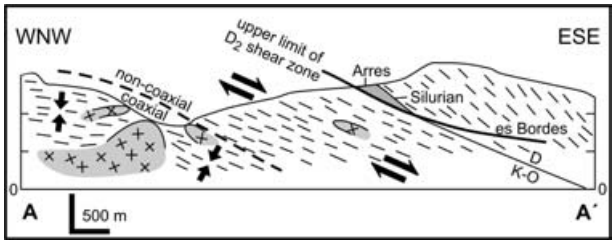


Figure 8. Schematic cross-section along the Garona river valley of the eastern part of the southern antiform. Solid and dashed thick lines mark the 1.5 km thick zone where non-coaxial $D_{2a}$ deformation with hanging wall-down sense of shear is preserved. Location of cross-section is shown on Figure 2.

around staurolite and domino boudin structures in biotite indicate the same sense of shear (Goscombe & Passchier, 2003). Staurolite is overgrown by centimetre-size andalusite porphybrolasts.

### 3.d. $D_{2b}$: non-coaxial deformation – $M_2$ contact metamorphism

Overprinting of $D_{2a}$ structures during $D_{2b}$ and the presence of low temperature phases, such as andalusite and cordierite, are indicative of a second distinct metamorphic event.

Andalusite commonly occurs in staurolite-bearing assemblages, where it forms prominent centimetre-size twinned poikiloblastic porphyroblasts with up to 50 vol. % inclusions of quartz, biotite and ilmenite. Inclusion trails have a convex symmetry, indicating vertical shortening of 25–50 %. Andalusite long axes are oriented parallel to $S_{1/2}$, and randomly within $S_{1/2}$. In sections perpendicular to crystal long axes, porphyroblasts have an oblate shape with width/height ratio of approximately 2. The abundance of andalusite is negatively correlated with that of staurolite (assemblage 3b). Andalusite is considered

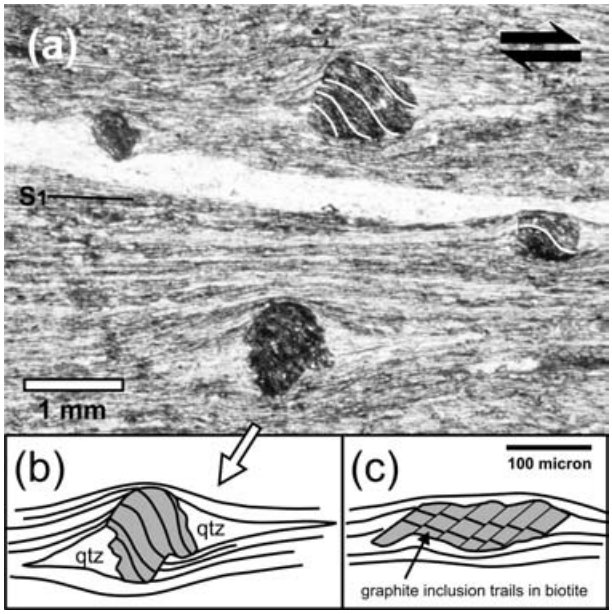


Figure 9. (a) Photomicrograph of a Devonian andalusite–staurolite–mica schist of the southeastern Bossòst dome near es Bordes. The section cut parallel to the mineral lineation shows staurolite porphyroblasts with a sigmoidal-shaped internal foliation of quartz and graphite inclusions. The symmetry of the curvature is consistent throughout the sample. The external schistosity is cross-cut obliquely by a quartz vein. The quartz vein is flattened where it is bounded by the staurolite porphyroblasts, indicating that ductile deformation continued after development of the vein. (Plane-polarized light.) (b) Sketch of the lower staurolite porphyroblast outlining the curved inclusion trails and quartz strain shadows. The inclusion patterns and the $\sigma$-type porphyroblast indicate dextral (top-to-the-right) sense of shear. (c) Sketch of a biotite fish with domino boudin structure and graphite inclusion trails oblique to the external foliation indicating the same sense of shear as rotated staurolite porphyroblasts.

to be the product of dehydration reactions that involve the breakdown of muscovite, chlorite and staurolite (reactions 3 and 4, Table 2). Centimetre-size andalusite porphyroblasts are also present in fine-grained chlorite–mica schist (assemblage 3a) distal to the granitic core in the northern part (Fig. 2).

Sillimanite occurs as fibrolite, rarely as prismatic sillimanite, within 500 m of exposed granites (assemblages 4a and 4b). Fibrolite is evenly distributed throughout the rock and grows epitaxially, parallel to the {001}-plane, on biotite. In contact with andalusite, fibrolite nucleates on biotite. Andalusite lacks textural signs of corrosion and does not show preferential growth of fibrolite along its grain boundaries, suggesting that fibrolite resulted from replacement of biotite instead of andalusite. Large poikiloblastic muscovites overgrowing cleavage domains are observed near fibrolitic lenses. Kerrick (1987) and Kerrick & Woodsworth (1989) proposed that fibrolite had formed from the decomposition of biotite, due to removal of K, Mg and Fe caused by acidic fluids

Table 2. Mineral reactions of the KFMASH, KFASH and FMASH systems relevant for the metamorphic evolution of the Cambro–Ordovician schist of the Bossòst dome

(1) muscovite + chlorite + quartz = almandine + annite + $H_2O$
(2) chlorite + muscovite = staurolite + biotite + quartz
(3) staurolite + chlorite + muscovite + quartz = aluminosilicate + biotite + $H_2O$
(4) chlorite + muscovite = aluminosilicate + biotite + quartz + $H_2O$
(5) chlorite + muscovite + quartz = biotite + cordierite + $H_2O$
(6) staurolite + quartz = cordierite + aluminosilicate + $H_2O$
(7) cordierite + muscovite = andalusite + biotite + quartz + $H_2O$
(8) chlorite + muscovite + quartz = aluminosilicate + biotite + cordierite + $H_2O$

References: (1) Bucher & Frey (1994, p. 202), (2) Deer, Howie & Zussman (1982, p. 849), (3) to (5) Pattison & Tracy (1991, p. 132, 136), (6) Deer, Howie & Zussman (1986, p. 474), (7), (8) Pattison, Spear & Cheney (1999).

that emanated from adjacent magmatic intrusions. Contemporaneous muscovite would act as a local K sink. In the Bossòst dome, complete replacement of biotite and coalescence across intermediate quartz-rich zones, where fibrolite grew without a preferred orientation, formed millimetre-long fibrolite lenses characterized by foliation-parallel needles at the margin and irregularly oriented needles in the centre. Spry (1969, p. 272) referred to this process as irregular growth of fibrolite following seeded nucleation. In contrast to Vernon (1987), who described samples from unspecified localities in the Bossòst area, the fibrolite lenses we observed did not show any evidence of residual crenulation folds or nucleation in zones of high non-coaxial strain. Fibrolite growth associated with shear zones has been observed in only one sample. The presence of deflected $S_{1/2}$ around the fibrolite lenses suggests that the lensoid shape resulted from coaxial deformation during coalescence.

Proximal to granitic intrusions, cordierite coexists with staurolite and garnet (assemblage 5b, Fig. 4c) or staurolite, garnet and andalusite (assemblage 5c) or staurolite, andalusite and sillimanite (assemblage 5d). Cordierite can contain inclusions of staurolite which show strongly corroded rims (Fig. 10a) that suggest consumption of staurolite to form cordierite and andalusite (reaction 6, Table 2). Cordierite pseudomorphs after lensoid andalusite, preserving convex inclusion trails and relics of andalusite, are observed as well. Biotite and ilmenite are common inclusions in cordierite, and while the matrix contains more biotite, ilmenite is rare (Fig. 4c). Since $TiO_2$ is abundant in biotite (*c*. 2 wt%), but occurs only as traces in cordierite, ilmenite formed from $TiO_2$ released by the breakdown of biotite to form cordierite. This reaction also consumed andalusite and produced muscovite, which can occur as large, randomly oriented muscovite porphyroblasts in the matrix (reaction 7, Table 2). The presence of coexisting cordierite, andalusite and staurolite, and evidence for corrosion of andalusite, suggest that the andalusite-producing reaction (4) had not been completed, when cordierite-producing reaction (7) began to consume andalusite. The lack of textural and chemical evidence for resorption at rims of garnet inclusions in cordierite indicates that garnet did not play a role in cordierite formation (Fig. 10a).

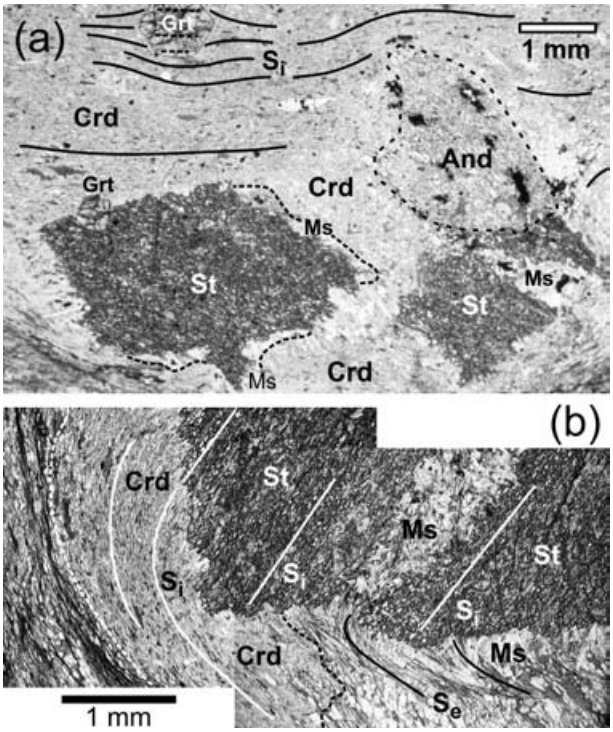


Figure 10. Photomicrographs of a garnet–staurolite–andalusite–cordierite schist (assemblage 5c). (a) Cordierite porphyroblast with inclusions of garnet, staurolite and andalusite. In contrast to the strongly corroded andalusite and staurolite grains, the garnet has retained its euhedral shape and is only slightly corroded. Staurolite grains are partially rimmed by coarse muscovite and are in contact with andalusite. $S_i$ in cordierite is deflected around garnet. (b) Detail of a staurolite porphyroblast mantled by muscovite and overgrown by cordierite (dashed line). Elongated quartz inclusions in the staurolite define straight $S_i$ (white line). At the grain boundary $S_i$ continues into $S_e$ (black line), defined by muscovite grains, which curves about 90°. On the left, cordierite porphyroblast completely replaced staurolite and parts of the mica strain cap, resulting in a curved $S_i$ within cordierite. This underscores the importance of the metamorphic growth sequence for interpretation of shear sense indicators. Sections oriented parallel to the $L_2$ mineral lineation. (Plane-polarized light.)

Alteration of cordierite to pinite, a fine intergrowth of muscovite and chlorite, is common. As an artefact of the former cordierite, Fe and Mg are more abundant in the muscovite derived from alteration than in the matrix muscovite.

Schlieren structures and disruption of $S_{1/2}$ schistosity, immediately west of the peak of Montlude, are indicative of migmatization, marking the highest metamorphic grade observed in the Bossòst dome (Fig. 2). Potassium-feldspar is observed in sillimanite–biotite–muscovite schist and cordierite–biotite–sillimanite gneiss (assemblage 5f). It is not clear, however, if potassium-feldspar is of metamorphic subsolidus origin or derived from the melt. Assemblage 5f marks the final disappearance of muscovite.

The restriction of cordierite and aluminosilicate-bearing assemblages to the proximity, generally within 1 km, of the granitic rocks suggests that contact metamorphism related to the intrusion of the granites was the cause of $M_2$. Fibrolitic sillimanite derived from cation leaching of biotite indicates the presence of nearby intruding magma (Kerrick, 1987). Fibrolite formed this way is inferred to be metastable within the andalusite stability field. The contact aureole has a thickness of approximately 500 m and is prominently developed in the northern section where it almost completely anneals the earlier $M_1$ paragenesis. There, only relics of staurolite remain.

Complete cordierite pseudomorphism after rotated staurolite porphyroblasts results in curved inclusion trails that could be misinterpreted as synkinematic growth of the cordierite porphyroblast (Fig. 10b), especially in outcrop. There is, however, evidence for late synkinematic growth of cordierite as indicated by curvature of $S_{1/2}$ inclusion trails at the rim and obliquity between $S_i$ in cordierite and in inclusions of biotite in cordierite, with the same asymmetry (Fig. 4c, e). Tilting of andalusite porphyroblasts in some andalusite schists can also be attributed to this late-$D_{2b}$ non-coaxial deformation. Locally developed C′-type shear bands with hanging wall-down-to-the-SE sense of shear are also inferred to be $D_{2b}$ fabrics.

The sense and direction of shear during $D_{2b}$ is the same as in $D_{2a}$ (Fig. 7). For this reason, we consider $D_{2a}$ and $D_{2b}$ as early and late stages of the same deformation phase. In the northern part of the area, $L_2$ may be the result of strong coaxial deformation in the contact aureole. Thus, the fan-shaped orientation of $L_2$ around the granitic intrusion (Fig. 2) could be an original feature and reflect flow away from the intrusive contact. This would indicate an age younger than that of the lineation in the southern antiform.

### 3.e. $D_3$: micro- to macro-scale folding

Millimetre-scale crenulation folding of $S_{1/2}$ is developed subparallel to $L_2$. Where trends of $L_2$ and crenulation fold axes can be distinguished, $L_2$ is folded by crenulations. Thin-sections cut perpendicular to $L_2$ show that crenulation bands initiate at the tip of staurolite and cordierite porphyroblasts and fold

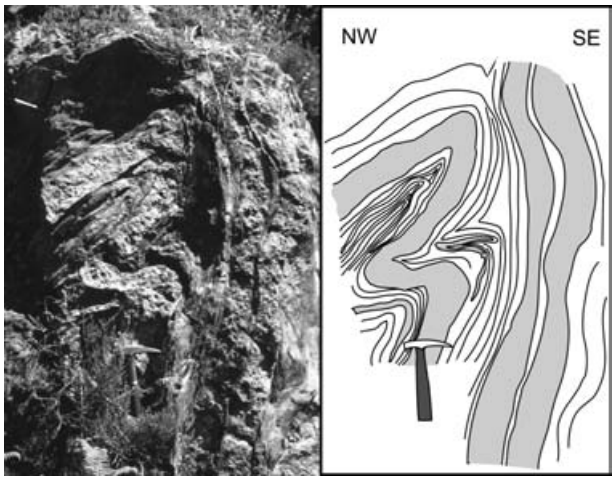


Figure 11. Asymmetrical tight folding of quartzitic mica schist with decimetre-thick granitic sills. The slightly overturned antiform verges towards the southeast. Road outcrop along Arrui de Varrados valley, immediately north of the Bossòst Fault. See Figure 2 for location. Hammer for scale is approximately 35 cm long.

fibrolitic sillimanite, suggesting that crenulation folds post-date $M_2$.

Open and close to tight folds with 0.1–2 m wavelengths and a general southerly vergence are common. These folds can display axial planar and layer-parallel discrete shear planes and blind thrusts with a southerly transport direction. Mesoscale folds and crenulations developed in the same rocks show parallel orientation of their axes, prohibiting establishment of their relative ages. $F_3$ fold axes south of the Bossòst Fault trend approximately ESE–WNW and plunge shallowly (Fig. 3). In the northern section, $F_3$ fold axis orientations display a regional variation similar to $L_2$. From W to E, plunge directions shift gradually from NE to SE. This may be attributed to local deviation of the stress field around a more rigid granite body. Folding of massive granitic sills just north of the Bossòst Fault indicates that $F_3$ folding post-dates the granite intrusion (Fig. 11). Similarly oriented crenulation and open folds are observed in the Devonian rocks in the Garona river valley.

Regional kilometre-scale $D_3$ folds affect $S_{1/2}$ throughout the Bossòst dome. In the northern section, regional $F_3$ folds are SSW-verging with subhorizontal ESE-trending fold axes. South of the Bossòst Fault, an ESE-trending syn- and antiform fold pair with 2 km wavelength is developed (Figs 2, 12). The folds are S-verging with moderately to steeply (45–60°) S-dipping and moderately (20–30°) N-dipping limbs. Fold axes plunge shallowly (*c.* 15°) to the ESE, subparallel to the orientation of the Bossòst Fault. The northern limb of the synform steepens towards the Bossòst Fault and tapers out westwards to the international border (Fig. 12). Towards the contact with the overlying Silurian and Devonian slates in the east, secondary

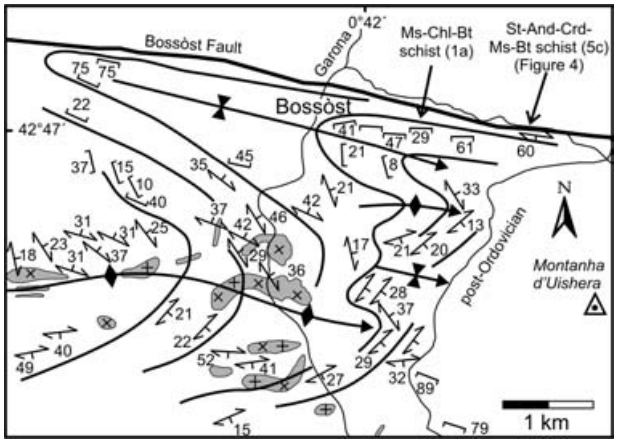


Figure 12. Detailed structural map of the central study area between the Bossòst Fault and the southern granite intrusions. Lines trace the $S_1$ foliation and outline the $F_3$ syn- and antiform pair. Subparallel secondary folds are developed in the Cambro-Ordovician rocks close to the contact with the overlying post-Ordovician slates. The high-grade assemblage 5c on the steep northern limb of the antiform immediately south of the Bossòst Fault is located structurally below the low-grade muscovite–chlorite–biotite schist to the west, indicating that folding post-dates intrusion. The structural symbols with dip angles are the same as in Figure 2.

asymmetrical folds are observed. The hinge zone of the southern antiform can be traced westward where it gradually changes from an ESE plunge to a horizontal and eventually shallow (8°) WNW-plunge south of Bàgneres de Luchon, forming a doubly plunging antiform (Fig. 2).

Associated with the $F_3$ folds, but not developed everywhere, is an ESE–WNW-striking, subvertical, millimetre- to centimetre-spaced discrete $S_3$ cleavage. In contrast to $S_3$ of Pouget (1991), we did not observe this cleavage to be confined to the proximity of granitic intrusions (Fig. 2).

Based on the parallelism of fold axes and an overall southerly vergence, we attribute development of the millimetre-scale crenulation folds, the outcrop scale folds and the regional folds to one major deformation phase (Fig. 4). The absolute age is difficult to determine due to the lack of datable cross-cutting events, but folded granite sills (Fig. 11) indicate a latest Variscan or younger age. The discordance with N-verging folds in the overlying Silurian and Devonian rocks reported by Garcia-Sansegundo (1996) implies that the NNE–SSW compression responsible for $F_3$ folds was active before the Alpine thrusting reported along the Gavarnie thrust in the Lys-Caillaouas massif to the southwest (de Bresser, Majoor & Ploegsma, 1986).

The parallel trace of the southern folds to the Bossòst Fault and steepening of the northern limb towards the fault may indicate initiation of the fault structure during development of the S-verging $F_3$ regional folds, possibly by southward-directed thrusting along a subvertical limb.

### 3.f. $D_4$: brittle folding

Centimetre- to decimetre-spaced kink folds are less common and are predominantly observed in slaty and schistose rocks of the northern part of the Bossòst dome. Their relative young age is indicated by brittle deformation of centimetre-sized andalusite porphyroblasts and deflection of $F_3$ crenulation folds. $F_4$ kink fold axes are subhorizontal and trend to ESE and WNW, subparallel to the direction of the mesoscopic and regional $F_3$ fold axes (Fig. 3). From the available data it is not possible to determine if $F_4$ kink folding reflects the late-stage NNE–SSW compression that formed $F_3$ folds or younger compressional events.

### 3.g. $D_5$

Subvertical, E- to SE-striking discrete shear zones 5 cm to 2 m wide cross-cut $S_{1/2}$ and are predominantly observed in the southwestern Bossòst dome. Similar orientation of the shear zones on the opposite limbs of the antiform suggests that the shear zones were developed after $D_3$ regional folding. These shear zones may correlate to Alpine age mylonite zones reported by C. Lamouroux (unpub. Ph.D. thesis, Univ. Toulouse, 1987, p. 51), although reliable geochronological data are not available. Alpine ages were obtained from $^{40}Ar/^{39}Ar$ geochronology on mylonites of the Merens Fault south of the Aston Massif, and from K–Ar and Rb–Sr geochronology of WNW–ESE-trending shear zones in the Aston orthogneiss by McCaig & Miller (1986) and F. J. M. Majoor (unpub. Ph.D. thesis, Univ. Amsterdam, 1988), but Variscan deformation could not be excluded.

## 4. *P–T* path

In the Bossòst area, two distinct phases of quasi-static porphyroblast growth are separated by a period of non-coaxial progressive deformation ($D_2$). During the first event, $M_1$, garnet and staurolite were formed. Microprobe analyses of ferro-magnesian phases (grt, st, crd, bt, ms) show an enrichment of Mn (5×) and Mg (2×) in samples with coexisting staurolite and cordierite with respect to a staurolite-only sample (00–165, Table 1). This indicates a difference in bulk rock composition that is reflected in garnet composition and has implications for the nucleation of garnet. The KFMASH petrogenetic grid in Figure 13 shows that staurolite (reaction 2) appears at lower temperatures than garnet (reaction 1). Textural evidence suggests this is the case for the Fe-rich ($X_{alm}$ 88) garnets of sample 00–165. In cordierite-bearing samples with Mn as a significant additional phase, garnet can begin to grow at considerably lower temperatures (*c.* 450 °C, Spear, 1993, p. 353), as evident from spessartine-rich ($X_{sps}$ 25) garnet inclusions in staurolite (Fig. 10a). The amount of pressure-sensitive Ca is equal in both

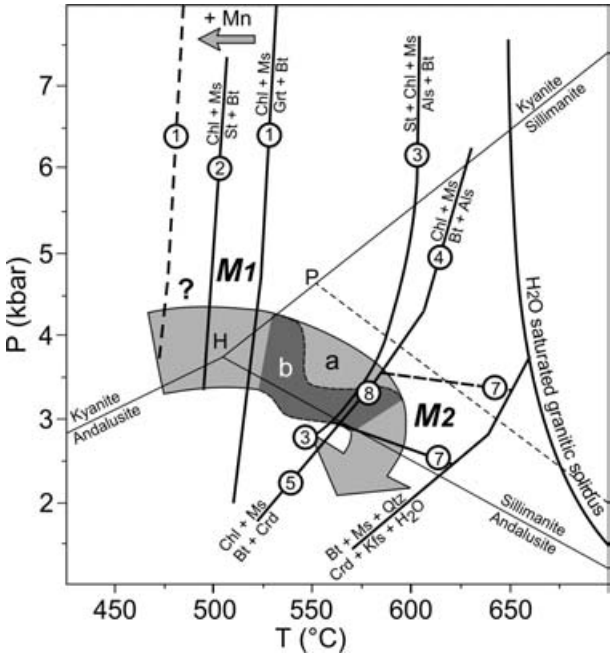


Figure 13. Petrogenetic grid of the KFMASH system relevant to the Cambro-Ordovician schist of the Bossòst dome and possible *P–T* paths. Numbers on curves refer to the reactions listed in Table 2. The shift of reaction (1) with Mn as an additional component to lower temperature is indicated by the dashed line. The locations of reaction (7), with respect to the aluminosilicate triple points of Holdaway & Mukhopadhyay (1993) (solid line) and Pattison (1992) (dashed line), are obtained from Pattison *et al.* (2002) for graphite-absent rocks and Mg/(Fe + Mg) of 0.48 in biotite. With $aH_2O$ in equilibrium with graphite, reaction (7) shifts 0.5 kbar to lower pressures. Path 'a' describes a continuous clockwise loop with decompression during heating, while 'b' follows a path of isothermal decompression, then isobaric heating. Als – aluminosilicate; Chl – chlorite; Kfs – K-feldspar; other abbreviations as in Figure 4.

assemblages. Fe/(Fe + Mg) values remain unchanged along a compositional traverse, suggesting that the temperature did not change significantly during garnet growth. Thus, the two different garnet compositions reflect different bulk rock compositions, which result in different growth successions of garnet and staurolite. They do not, however, indicate significantly different metamorphic grades, for example, medium and low pressure, as suggested by Pouget (1991).

The absence of kyanite or sillimanite as a result of staurolite breakdown, associated with $M_1$, suggests that temperatures did not exceed 600 °C (Fig. 13). Electron microprobe analyses of two biotite generations did not reveal compositional differences, which can be explained by re-equilibration during subsequent metamorphic events or cooling. Furthermore, lack of evidence for resorption of garnet during later events strongly suggests chemical disequilibrium between garnet and biotite. Thus, they cannot be used for geothermometry. The high temperatures (> 650 °C) calculated by Pouget (1991) would have caused diffusion-driven chemical homogenization of low-temperature spessartine garnets, and this is not observed. The pressure during the early phase cannot be estimated, since pressure sensitive phases, plagioclase or aluminosilicates, are missing. Pouget (1991) used an uncommon staurolite–garnet barometer (Perchuck, 1977), which had not been tested elsewhere. Without additional independent evidence, his calculated pressure conditions of 6 kbar cannot be considered reliable. We propose a minimum pressure of approximately 3 kbar, equivalent to bathozone 3 of Carmichael (1978).

$M_2$ is characterized by the successive overprinting of rotated staurolite and garnet porphyroblasts by andalusite and cordierite (Fig. 10). Corroded inclusions of andalusite in cordierite indicate that cordierite is younger than andalusite. Cordierite–staurolite–muscovite–biotite assemblages (5b and 5c) are considered metastable and the result of polymetamorphism (Holdaway *et al.* 1982; Garcia-Casco & Torres-Roldán, 1999). Pattison, Spear & Cheney (1999) concluded that if combined (Mn + Zn)/(Fe + Mg + Mn + Zn) in coexisting cordierite and staurolite does not exceed 0.15, the Ms + Crd + St + Bt stability field would be too small to occur frequently in natural samples. In the Bossòst samples the ratios are 0.08 and 0.15 (Table 1). On the KFMASH grid of Figure 13 these rocks would pass through reactions (3) and (4) to form andalusite and along a decompression path through reaction (7), which has a shallow negative slope, to form cordierite after andalusite (Pattison *et al.* 2002). Several factors control the location of reaction (7): the applied sillimanite–andalusite equilibrium model, the Mg/Fe ratio of biotite and the presence of graphite. Figure 13 depicts the location of reaction (7) using average Mg/(Fe + Mg) ratios for biotite of the Bossòst samples. Graphite is not abundant and was omitted in the calculation. Applying the common aluminosilicate triple point models of Pattison (1992) and Holdaway & Mukhopadhyay (1993), reaction (7) lies close to the sillimanite–andalusite equilibrium. With additional graphite, the location of reaction (7) shifts to lower pressures. The textural relationships and porphyroblast growth sequences observed in the Bossòst dome correspond to muscovite–cordierite–staurolite–biotite assemblages discussed by Pattison, Spear & Cheney (1999) and Pattison *et al.* (2002), strongly suggesting a polymetamorphic origin of the Bossòst assemblages.

The growth of cordierite after andalusite implies a component of decompression, whose magnitude is difficult to assess, since pressure conditions for $M_1$ are poorly constrained. For that reason, end-member *P–T* paths can be postulated, as shown in Figure 13. Path (a) is a general clockwise loop with heating during decompression, while path (b) depicts isothermal decompression followed by isobaric heating. Peak temperatures during $M_2$ were approximately 575–600 °C at 3 kbar.

## 5. Tectonic model

Garnet and staurolite porphyroblasts overgrew an existing flat-lying $S_1$ schistosity during a period of deformational quiescence. There is no evidence that $S_1$ was transformed from an originally older steeply dipping foliation, as postulated by Pouget (1991). Our observations are in agreement with Matte (1969), García-Sansegundo & Alonso (1989) and García-Sansegundo (1996), who suggested that the oldest tectonic foliation is a flat-lying cleavage axial planar to large W-vergent recumbent folds. This recumbent folding occurred during the mid-Westphalian age (*c.* 310 Ma: Matte & Xu Zhi, 1988) and resulted in crustal thickening (Fig. 14a). During crustal thickening the flat-lying schistosity was formed and the thermal isograds were deflected downward. Static overgrowth of $S_{1/2}$ by garnet and staurolite indicates a delay of peak regional metamorphic conditions due to subsequent thermal relaxation within the thickened crust (Fig. 14b). An exception are low-temperature spessartine garnets with crenulated inclusion trails, which indicate growth prior to complete formation of $S_{1/2}$. Lacking suitable mineral parageneses for geobarometry, the minimum pressure of staurolite formation must exceed that of the cordierite-forming reaction (7), which is crossed at 3 kbar during decompression (Fig. 13).

Non-coaxial $D_{2a}$ deformation with top-to-the-ESE sense of shear is preserved in a 1.5 km thick zone in the western part of the southern antiform (Fig. 14c). Deformation apparently became more coaxial at the onset of $M_2$ contact metamorphism, as evident from cordierite overprinting the rotated staurolite porphyroblast. The distinct separation of $M_1$ and $M_2$ in the Cambro-Ordovician schist by non-coaxial deformation suggests that the $D_{2a}$ shear zone facilitated uplift of the core zone of the Bossòst dome in a system of regional extension. The exact amount of uplift cannot be established due to the lack of reliable pressure estimates for $M_1$. Though there is no geochronological evidence, initiation of $D_{2a}$ extensional shearing could have occurred during the period of thermal relaxation that led to $M_1$ regional metamorphism. At the same time, granitic melt of the main intrusion could have begun to form at lower structural levels. Vissers (1992) and Aerden (1994) proposed gravity collapse of a thickened lithosphere as reason for granitic emplacement in other metamorphic domes of the Axial Zone. Initiation of the domal shape of the Bossòst structural dome occurred with the intrusion of the granite and preceded $F_3$ folding. The absence of a significant amount of migmatized Cambro-Ordovician metasedimentary rocks suggests that granitic magma did not melt *in situ*, but intruded the country rocks (Fig. 14d). In the northern part the intrusion forms a batholith, and vertical shortening is recorded in convex inclusion trails in andalusite porphyroblasts within the surrounding $M_2$ contact aureole. In the southern part the intrusions appear to be controlled by $S_{1/2}$ fabrics, forming sills and dykes, with coaxial deformation near the intrusive contacts, but also non-coaxial shearing within the $D_{2a}$ shear zone, as indicated by the late synkinematic growth phase of cordierite (Fig. 4c).

Replacement of andalusite by cordierite occurred along a decompression path, suggesting that $M_2$ contact

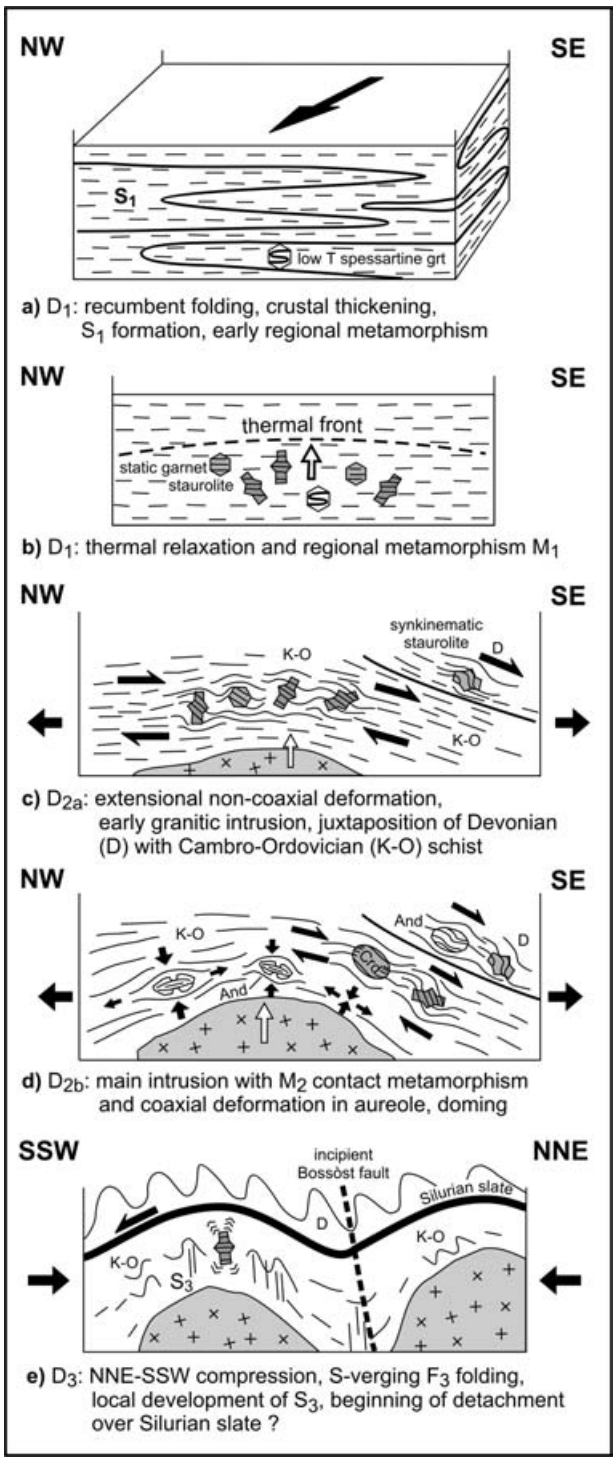


Figure 14. Proposed tectonic model for the development of the Bossòst dome. Not to scale. Note that section (e) is normal to the previous sections.

metamorphism was not static but continued during uplift. This suggests that $D_2$ was a period of continuous non-coaxial deformation, with dominance of more coaxial deformation in the immediate contact aureole. In fact, the narrow contact aureole and the strongly poikiloblastic nature of andalusite and cordierite suggest fast growth of these phases within the deformational time frame. Synkinematic staurolite and andalusite in the Devonian schist near es Bordes indicate close temporal relation between $M_1$, $D_{2a}$ and $M_2$ (Fig. 10). Considering the proposed ages for $D_1$ recumbent folding, mid-Westphalian age (*c*. 310 Ma: Matte & Xu Zhi, 1988), and intrusion of granitic plutons of the eastern Axial Zone (312–305 Ma: Gleizes, Leblanc & Bouchez, 1997), regional and contact metamorphism should have occurred almost simultaneously.

The geometries of the intrusions may reflect different erosional levels of the northern and southern parts, however, it is difficult to prove on the basis of petrological evidence alone. The intrusions in the two parts of the dome appear to represent two separate magmatic bodies.

The initiation of $F_3$ crenulation folds on staurolite and cordierite porphyroblasts and folding of granitic sills indicate that NNE–SSW-directed $D_3$ compression post-dates the $D_2$ non-coaxial deformation and granitic intrusion with related $M_2$ contact metamorphism. Interference of E-trending metamorphic culminations and NNE–SSW shortening created the doubly plunging antiform–synform structures (Fig. 14e). The strong metamorphic contrast between Cambro-Ordovician schist and overlying Silurian and Devonian slate originated during the extensional uplift of the schist along the $D_{2a}$ extensional shear zone. During $D_3$, low competent post-Ordovician metasedimentary rocks formed tighter folds than the underlying schists, which caused decoupling along a southward-directed décollement within the soft Silurian black slate (Matte & Xu Zhi, 1988). Additional thrusting may be correlative to postulated Alpine thrusting along the Gavarnie thrust in the Lys-Caillaouas massif to the southwest (de Bresser, Majoor & Ploegsma, 1986).

## 6. Discussion

Two discrete periods of metamorphism in Cambro-Ordovician rocks are separated by intense non-coaxial deformation: (1) a medium-*P*–medium-*T* regional metamorphism $M_1$ that statically overprinted an existing $S_1$ schistosity; (2) a relative low-*P*–high-*T* contact metamorphism $M_2$ coeval with general coaxial deformation. Kilometre-scale uplift of the metamorphic core of the Bossòst dome occurred along an ESE-directed extensional shear zone. This shear zone is located in the southeastern part of the dome, where it preserved a structural thickness of 1.5 km. It is difficult to estimate the original dimensions of that shear zone. Later granitic intrusion with associated contact metamorphism, N–S compression and possible Alpine thrusting may have obliterated possible evidence for the shear zone elsewhere in the dome. However, van den Eeckhout & Zwart (1988) proposed a 4 km thick crustal-scale shear zone of similar orientation and temporal relationship with the main deformational and intrusive events to be located within Cambro-Ordovician schist immediately overlying the Hospitalêt gneiss dome.

Without reliable geochronological data, the timing and duration of the shear zone is also difficult to assess. Assuming a mid-Westphalian (*c*. 310 Ma) age for $S_1$ formation and granite intrusion at approximately 300 Ma, the emplacement age of most plutons in the Axial Zone (Gleizes, Leblanc & Bouchez, 1997), the main deformation events occurred in a restricted time frame. Supporting evidence is seen in the Devonian schist where $D_{2a}$ and $M_2$ overlap.

Parallelism of the stretching lineation with fold axes around dome structures is viewed by Matte, Lancelot & Mattauer (1998) as the result of dome-parallel shearing coeval with folding in a bulk compressional setting. Fletcher *et al.* (1995) proposed that extension-parallel folding can result from horizontal stress perpendicular to the extensional direction within a thinned crust in a general extensional setting. In the Bossòst dome, however, $F_3$ folds clearly post-date non-coaxial deformation and no causal relationship can be inferred.

Carreras & Capella (1994) have described the complex inhomogeneities of deformation throughout the Variscan tectonic history of the Axial Zone and cautioned against correlating structures across the orogen. Development of flat or steep structures in the infrastructure can depend on dominance of flat- or wrench-shearing. Rheological heterogeneities, for example, pre-Variscan gneiss domes, such as the Aston-Hospitalêt and the Canigou massifs, can result in strain partitioning during the main Variscan deformation. Gleizes, Leblanc & Bouchez (1997) reported diachronous emplacement of late Variscan plutons with respect to the main deformation phase.

Taking this into account, the Bossòst dome is interpreted to be the result of two compressional events separated by a temporally restricted phase of dome-subparallel extension. This extension may have also been restricted spatially due to strain partitioning and occurred during bulk compression. Observations from other structural domes indicate that extension occurred throughout the Axial Zone (van den Eeckhout & Zwart, 1988; Bon *et al.* 1994). However, our study of the Bossòst dome does not support Vissers' (1992) notion that crustal extension was the last major Variscan deformational event. Furthermore, we find no evidence in this area for major dextral transpression during $D_2$ which was inferred from pre- and synkinematic emplacements of late Variscan plutons in the eastern Axial zone (Gleizes, Leblanc & Bouchez, 1997).

**Acknowledgements.** Research was supported by the Deutsche Forschungsgemeinschaft as part of the Graduiertenkolleg "Stoffbestand und Entwicklung von Kruste und Mantel" (JEM) and grant PA 578/5-1 (CWP). Discussions with Jordi Carreras and Bas van den Eeckhout were inspiring. Roger Gibson, Philippe Matte and Andrew McCaig are thanked for their constructive reviews.

## References

AERDEN, D. G. A. M. 1994. Kinematics of orogenic collapse in the Variscan Pyrenees deduced from microstructures in porphyroblastic rocks from the Lys-Caillaouas massif. *Tectonophysics* **238**, 139–60.

AERDEN, D. G. A. M. 1998. Tectonic evolution of the Montagne Noir and a possible orogenic model for syncollisional exhumation of deep rocks, Variscan belt, France. *Tectonics* **17**, 62–79.

BARBEY, P., CHEILLETZ, A. & LAUMONIER, B. 2001. The Canigou orthogneiss (Eastern Pyrenees, France, Spain): an Early Ordovician rapakivi granite laccolith and its contact aureole. *Comptes Rendus de l'Académie des Sciences* **332**, 129–36.

BARTHOLOMÉ, P. 1953. Sur la structure du massif granitique de Bosost-Val d'Aran d'Espagne. *Annales Societé Géologique de Belgique* **76**, 317–28.

BELL, T. H. & RUBENACH, M. J. 1983. Sequential porphyroblast growth and crenulation cleavage development during progressive deformation. *Tectonophysics* **92**, 171–94.

BON, A., VAN DEN EECKHOUT, B., JANZEN, E., KLEPPER, C., VAN MOERKERKEN, B. & VAN WEES, J. D. 1994. Timing of Variscan mid-crustal shearing and batholith intrusion in the Central Pyrenees (Ariège, France). *Geologie en Mijnbouw* **73**, 53–61.

BUCHER, K. & FREY, M. 1994. *Petrogenesis of Metamorphic Rocks.* Berlin, New York: Springer Verlag, 318 pp.

CALEMBERT, L. 1951. Sur la géologie des environs de Bosost (hautes Pyrénées d'Espagne). *Annales Societé Géologique de Belgique* **75**, 123–30.

CARMICHAEL, D. M. 1978. Metamorphic bathozones and bathograds: a measure of the depth of post-metamorphic uplift and erosion on the regional scale. *American Journal of Science* **278**, 769–97.

CARRERAS, J. & CAPELLA, I. 1994. Tectonic levels in the Palaeozoic basement of the Pyrenees: a review and new interpretation. *Journal of Structural Geology* **16**, 1509–24.

DE BRESSER, J. H. P., MAJOOR, F. J. M. & PLOEGSMA, M. 1986. New insights in the structural and metamorphic history of the western Lys-Caillauas massif (Central Pyrenees, France). *Geologie en Mijnbouw* **65**, 177–87.

DEER, W. A., HOWIE, R. A. & ZUSSMAN, J. 1982. *Orthosilicates.* 2nd ed. London: Longman, 919 pp.

DEER, W. A., HOWIE, R. A. & ZUSSMAN, J. 1986. *Disilicates and Ring Silicates.* 2nd ed. London: Longman, 629 pp.

DELOULE, E., ALEXANDROV, P., CHEILLETZ, A., LAUMONIER, B. & BARBEY, P. 2002. In-situ U-Pb zircon ages for Early Ordovician magmatism in the Eastern Pyrenees, France: the Canigou orthogneisses. *International Journal of Earth Sciences* **91**, 398–405.

DE SITTER, L. U. & ZWART, H. J. 1960. *Geological map of the Central Pyrenees, sheet 4 Valle de Aran, Spain, 1:50,000.* Geological Institute, University of Leiden.

DIRKS, P. H. M., ZHANG, J. S. & PASSCHIER, C. W. 1997. Exhumation of high-pressure granulites and the role of lower crustal advection in the North China Craton near Datung. *Journal of Structural Geology* **19**, 1343–58.

ESKOLA, P. E. 1949. The problem of mantled gneiss domes. *Quarterly Journal of the Geological Society of London* **104**, 461–76.

EVANS, N. G., GLEIZES, G., LEBLANC, D. & BOUCHEZ, J. L. 1998. Syntectonic emplacement of the Maladeta granite (Pyrenees) deduced from relationships between Hercynian deformation and contact metamorphism. *Journal of the Geological Society, London* **155**, 209–16.

FLETCHER, J. M., BARTLEY, J. M., MARTIN, M. W., GLAZNER, A. F. & WALKER, J. D. 1995. Large-magnitude continental extension: An example from the central Mojave metamorphic core complex. *Geological Society of America Bulletin* **107**, 1468–83.

GARCÍA-CASCO, A. & TORRES-ROLDÁN, R. L. 1999. Natural metastable reactions involving garnet, staurolite and cordierite: Implications for petrogenetic grids and the extensional collapse of the Betic-Rif Belt. *Contributions to Mineralogy and Petrology* **136**, 131–53.

GARCIA-SANSEGUNDO, J. 1996. Hercynian structure of the Axial Zone of the Pyrenees: the Aran Valley cross-section (Spain-France). *Journal of Structural Geology* **18**, 1315–25.

GARCIA-SANSEGUNDO, J. & ALONSO, J. L. 1989. Stratigraphy and structure of the southeastern Garona Dome. *Geodinamica Acta* **3**, 127–34.

GIBSON, R. L. 1989. The relationship between deformation and metamorphism in the Carnigou Massif, Pyrenees: a case study. *Geologie en Mijnbouw* **68**, 345–56.

GIBSON, R. L. 1991. Hercynian low-pressure-high-temperature regional metamorphism and subhorizontal foliation development in the Canigou massif, Pyrenees, France - Evidence for crustal extension. *Geology* **19**, 380–3.

GIBSON, R. L. 1992. Discussion on Hercynian tectonometamorphic evolution of the Bosost dome (French-Spanish central Pyrenees). *Journal*, vol. 148, pp. 299–314: Comment. *Journal of the Geological Society, London* **149**, 156–7.

GLEIZES, G., LEBLANC, D. & BOUCHEZ, J. L. 1997. Variscan granites of the Pyrenees revisited: their role as syntectonic markers of the orogen. *Terra Nova* **9**, 38–41.

GOSCOMBE, B. D. & PASSCHIER, C. W. 2003. Asymmetric boudins as shear sense indicators – an assessment of field data. *Journal of Structural Geology* **25**, 575–89.

HETZEL, R., PASSCHIER, C. W., RING, U. & DORA, O. O. 1995. Bivergent extension in orogenic belts: the Menderes massif (southwest Turkey). *Geology* **23**, 455–8.

HOLDAWAY, M. J., GUIDOTTI, C. V., NOVAK, J. M. & HENRY, W. E. 1982. Polymetamorphism in medium- to high-grade pelitic metamorphic rocks, west-central Maine. *Geological Society of America Bulletin* **93**, 572–84.

HOLDAWAY, M. J. & MUKHOPADHYAY, B. 1993. Geothermobarometry in pelitic schists: A rapidly evolving field. *American Mineralogist* **78**, 681–93.

KERRICK, D. M. 1987. Fibrolite in contact aureoles of Donegal, Ireland. *American Mineralogist* **72**, 240–54.

KERRICK, D. M. & WOODSWORTH, G. J. 1989. Aluminum silicates in the Mount Raleigh pendant, British Columbia. *Journal of Metamorphic Geology* **7**, 547–63.

KRETZ, R. 1983. Symbols for rock-forming minerals. *American Mineralogist* **68**, 277–9.

KRIEGSMAN, L. M., AERDEN, D. G. A. M., BAKKER, R. J., DEN BROK, S. W. J. & SCHUTJENS, P. M. T. M. 1989. Variscan tectonometamorphic evolution of the eastern Lys-Caillaouas massif, Central Pyrenees - evidence for late orogenic extension prior to peak metamorphism. *Geologie en Mijnbouw* **68**, 323–33.

LAUMONIER, B. & AUTRAN, A. 2001. Un chevauchement hercynien majeur dans les Pyrénées orientales: le chevauchement du Puigmal. *Comptes Rendus de l'Académie des Sciences* **332**, 585–94.

LEBLANC, D., GLEIZES, G., ROUX, L. & BOUCHEZ, J. L. 1996. Variscan dextral transpression in the French Pyrenees: new data from the Pic des Trois-Seigneurs granodiorite and its country rocks. *Tectonophysics* **261**, 331–45.

LISTER, G. S. & DAVIS, G. A. 1989. The origin of metamorphic core complexes and detachment faults formed during Tertiary continental extension in the northern Colorado River region, U.S.A. *Journal of Structural Geology* **11**, 65–94.

MALAVIELLE, J., GUIHOIT, P., COSTA, S., LARDEAUX, J. M. & GARDIEN, V. 1990. Collapse of the thickened Variscan crust in the French Massif Central: Mont Pilat extensional shear zone and St. Etienne late Carboniferous basin. *Tectonophysics* **177**, 139–49.

MATTE, P. 1969. Le problème du passage de la schistosité horizontal à la schistosité verticale dans la dôme de la Garonne (Paléozoique des Pyrénées Centrales). *Comptes Rendus de l'Académie des Sciences* **268**, 1841–4.

MATTE, P. 2002. Les plis hercyniens kilométriques couchés vers l'ouest-sud-ouest dans la région du pic du Midi d'Ossau-col du Somport (zone axiale des Pyrénées occidentales). *Comptes Rendus de l'Académie des Sciences* **334**, 773–9.

MATTE, P., LANCELOT, J. & MATTAUER, M. 1998. La zone axiale hercynienne de la Montagne Noire n'est pas un "metamorphic core complex" extensif mais un anticlinal post-nappe à coeur anatectique. *Geodinamica Acta* **11**, 13–22.

MATTE, P. & XU ZHI, Q. 1988. Decollements in slate belts, examples from the European variscides and the Qin Lin Belt of Central China. *Geologische Rundschau* **77**, 227–38.

MCCAIG, A. M. & MILLER, J. A. 1986. $^{40}$Ar-$^{39}$Ar age of mylonites along the Merens fault, central Pyrenees. *Tectonophysics* **129**, 149–72.

MYERS, J. S. 1995. The generation and assembly of an Archean supercontinent: evidence from the Yilgarn craton, Western Australia. In *Early Precambrian Processes* (eds M. P. Coward and A. C. Ries), pp. 143–54. Geological Society of London, Special Publication no. 95.

OLIVER, G. J. H. 1994. Mid-Crustal detachment and domes in the central zone of the Damaran orogen, Namibia. *Journal of African Earth Sciences* **19**, 331–44.

PASSCHIER, C. W. 1994. Tectonic evolution of the eastern Yilgarn Craton, W-Australia: constraints from structures in the Leonora area. *Precambrian Research* **68**, 43–64.

PASSCHIER, C. W. & SPECK, P. J. 1994. The kinematic interpretation of obliquely transected porphyroblasts: an example from the Trois Seigneurs Massif, France. *Journal of Structural Geology* **16**, 971–84.

PASSCHIER, C. W., TROUW, R. A. J., ZWART, H. J. & VISSERS, R. L. M. 1992. Porphyroblast rotation: eppur si muove? *Journal of Metamorphic Geology* **10**, 283–94.

PATTISON, D. R. M. 1992. Stability of Andalusite and Sillimanite and the $Al_2SiO_5$ Triple Point: Constraints from the Ballachulish Aureole, Scotland. *Journal of Geology* **100**, 423–46.

PATTISON, D. R. & TRACY, R. J. 1991. Phase Equilibria and Thermobarometry of Metapelites. In *Contact Metamorphism* (ed. D. M. Kerrick), pp. 105–206. Mineralogical Society of America, Reviews in Mineralogy no. 26.

PATTISON, D. R. M., SPEAR, F. S. & CHENEY, J. T. 1999. Polymetamorphic evolution of muscovite + cordierite + staurolite + biotite assemblages: implications for the metapelitic petrogenetic grid and for P-T paths. *Journal of Metamorphic Geology* **17**, 685–703.

PATTISON, D. R. M., SPEAR, F. S., DEBUHR, C. L., CHENEY, J. T. & GUIDOTTI, C. V. 2002. Thermodynamic modelling of the reaction muscovite + cordierite -> $Al_2SiO_5$ + biotite + quartz + $H_2O$: constraints from natural assemblages and implications for the metapelitic petrogenetic grid. *Journal of Metamorphic Geology* **20**, 99–118.

PERCHUCK, L. L. 1977. Thermodynamic control of metamorphic processes. In *Energetics of geological processes* (eds S. K. Saxena and S. Bhattacharji), pp. 285–352. Heidelberg: Springer-Verlag.

POUGET, P. 1991. Hercynian tectonometamorphic evolution of the Bosost dome (French-Spanish central Pyrenees). *Journal of the Geological Society, London* **148**, 299–314.

RAMBERG, H. 1980. Diapirism and gravity collapse in the Scandinavian Caledonides. *Journal of the Geological Society, London* **137**, 261–70.

SOULA, J.-C. 1982. Characteristics and mode of emplacement of gneiss domes and plutonic domes in central-eastern Pyrenees. *Journal of Structural Geology* **19**, 29–41.

SPEAR, F. S. 1993. *Metamorphic Phase Equilibria and Pressure-Temperature-Time Paths.* Washington, D. C.: Mineralogical Society of America, 799 pp.

SPRY, A. 1969. *Metamorphic Textures.* Oxford: Pergamon, 350 pp.

TEYSSIER, C. & WHITNEY, D. L. 2002. Gneiss domes and orogeny. *Geology* **30**, 1139–42.

VAN DEN EECKHOUT, B. & ZWART, H. J. 1988. Hercynian crustal-scale extensional shear zone in the Pyrenees. *Geology* **16**, 135–8.

VERHOEF, P. N. W., VISSERS, R. L. M. & ZWART, H. J. 1984. A new interpretation of the structural and metamorphic history of the western Aston Massif (Central Pyrenees, France). *Geologie en Mijnbouw* **63**, 399–410.

VERNON, R. H. 1987. Growth and concentration of fibrous sillimanite related to heterogeneous deformation in K-feldspar-sillimanite metapelites. *Journal of Metamorphic Geology* **5**, 51–68.

VISSERS, R. L. M. 1992. Variscan extension in the Pyrenees. *Tectonics* **11**, 1369–84.

ZEGERS, T. E., DE KEIJZER, M., PASSCHIER, C. W. & WHITE, S. H. 1998. The Mulgandinnah Shear Zone: an Archean crustal strike-slip zone, Pilbara, Western Australia. *Precambrian Research* **88**, 233–47.

ZWART, H. J. 1962. On the determination of polymetamorphic mineral associations, and its application to the Bosost area (Central Pyrenees). *Geologische Rundschau* **52**, 38–65.

ZWART, H. J. 1963. The structural evolution of the Paleozoic of the Pyrenees. *Geologische Rundschau* **53**, 170–205.

ZWART, H. J. 1986. The Variscan orogeny of the Pyrenees. *Tectonophysics* **129**, 9–27.